Optical-nanofiber-based interface for single molecules

Sarah M. Skoff,[1,*] David Papencordt,[1] Hardy Schauffert,[1] Bernhard C. Bayer,[2] and Arno Rauschenbeutel[1,†]

[1]*Vienna Center for Quantum Science and Technology, Institute of Atomic and Subatomic Physics, Vienna University of Technology, Stadionallee 2, A-1020 Vienna, Austria*

[2]*Electron Microscopy Group, Faculty of Physics, University of Vienna, Boltzmanngasse 5, A-1090 Vienna, Austria*

Optical interfaces for quantum emitters are a prerequisite for implementing quantum networks. Here, we couple single molecules to the guided modes of an optical nanofiber. The molecules are embedded within a crystal that provides photostability and, due to the inhomogeneous broadening, a means to spectrally address single molecules. Single molecules are excited and detected solely via the nanofiber interface without the requirement of additional optical access. In this way, we realize a fully fiber-integrated system that is scalable and may become a versatile constituent for quantum hybrid systems.

I. INTRODUCTION

In recent years, single molecules in solids [1–7] and other solid-state quantum emitters such as color centers in diamond [8–11] and quantum dots [12–16] have gained increasing interest as building blocks for quantum networks [17,18], quantum metrology [19–21], and nanosensors [22–24]. For all these applications a strong light-matter interaction is essential. This can be achieved by coupling to a large ensemble of quantum emitters [25,26], by employing a cavity [27–30], or by decreasing the mode area of the interacting light field [31–36] and hence achieving a significant overlap between the absorption cross section of the emitter and the respective light field. A versatile platform to achieve such a small mode area of the light field are optical nanofibers [34,37]. An optical nanofiber is the waist of a tapered optical fiber (TOF) and has a diameter smaller than the wavelength of the light it is guiding. Therefore, an appreciable fraction of the light propagates outside the fiber in the form of an evanescent wave. Due to the strong transverse confinement of the light field, which prevails over the entire length of the nanofiber, the interaction with emitters close to the surface can be significant [33,38–41].

Single molecules in crystalline solids are efficient quantum emitters that exhibit strong zero phonon lines (ZPLs), which can be lifetime limited and as narrow as tens of megahertz at cryogenic temperatures [42,43]. Due to inhomogeneous broadening caused by the host crystal, such molecules can be spectrally discerned and individually addressed using a narrow-band laser [44]. For a low concentration of molecules, this makes it possible to circumvent the additional spatial selection that has been used for numerous single-molecule experiments in the past [45,46], even if a large fraction of the crystal is illuminated. This was also exploited in recent experiments [31,47], where single dibenzoterrylene molecules were coupled to light propagating through a nanocapillary.

Single molecules come in a large variety and they are small quantum emitters, which is useful when coupling them to nano- and microcavities [48–50] and also offers the possibility to study collective phenomena of quantum emitters. Additionally, single molecules such as polycyclic aromatic hydrocarbons can be spectrally very stable and do not suffer from photobleaching when embedded in the right host matrix. In addition to a near-unity quantum yield, these are very important features when working with solid-state emitters. Here, we show for the first time that single organic molecules can be interfaced with an optical nanofiber. This presents a new platform based on solid-state emitters that can be used for quantum optics and that is naturally integrated into optical fiber networks.

II. EXPERIMENTAL SETUP

In our experimental setup, the TOF resides inside a cryostat [Fig. 1(a)] and we interface terrylene molecules in a *para*-terphenyl (*p*-terphenyl) crystal with the evanescent light field surrounding its nanofiber. The latter has a total length of 3 mm and a diameter of 320 nm. The TOF is produced in a heat-and-pull process using a custom-made pulling rig [51]. In the 6.8-cm-long tapered section of the fiber, the weakly guided LP_{01} mode of the standard single-mode optical fiber is adiabatically transformed into the strongly guided HE_{11} mode of the nanofiber waist and back, yielding transmission losses of less than 2% from 520 to 650 nm. For our purpose, a broadband transmission is crucial as the excitation and detection wavelengths can differ by more than 100 nm. This requires a careful choice of tapering angles and waist diameter [52]. Terrylene in *p*-terphenyl can exhibit four different electronic transition frequencies from the ground to the first excited state, termed X1–X4, corresponding to four possible orientations of the molecules in the crystal. Molecules in the X4 orientation are resonant with light at 577.9 nm and have been shown to be very photostable [53]. Hence, all measurements presented here use molecules in this site. A simplified level diagram is depicted in Fig. 1(b). The laser excites the molecule on the zero phonon line 00ZPL that connects the ground and the

*sarah.skoff@tuwien.ac.at

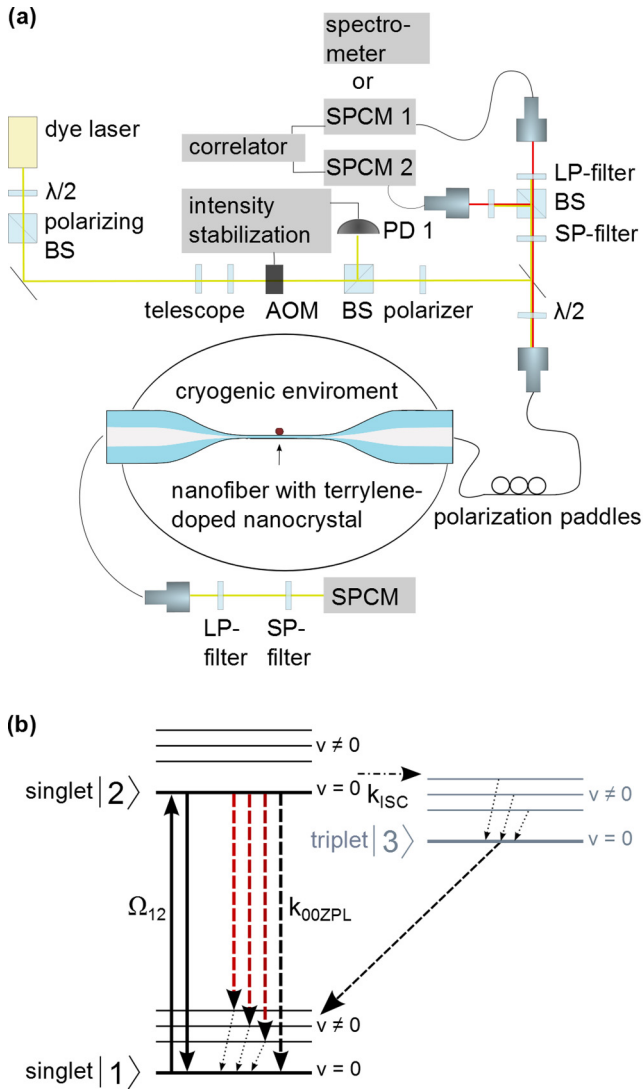†arno.rauschenbeutel@tuwien.ac.at

(a)

(b)

FIG. 1. (a) Experimental setup for single-molecule spectroscopy via an optical nanofiber interface. (b) Simplified level diagram of terrylene in *p*-terphenyl. Solid lines indicate transitions driven by the laser, while dashed lines represent spontaneous emission. The dot-dashed line marked k_{ISC} shows intersystem crossing from the excited singlet state to the triplet state. Dotted lines within an electronic manifold correspond to nonradiative decay processes that occur on a timescale of picoseconds.

excited electronic states without any vibrational contribution of the molecule. After excitation, the molecule will decay into any of the vibrational states in the electronic ground state with a probability determined by the Franck-Condon α_{FC} and Debye-Waller α_{DW} factors. From these states it will nonradiatively decay into the vibrational ground state within picoseconds. Hence, the absorption cross section [54] of a single molecule in a solid is

$$\sigma = \alpha_{FC}\,\alpha_{DW}\,\frac{3\lambda^2}{2\pi}\,\frac{\Gamma^2}{\Gamma_{hom}^2}(\hat{\mathbf{d}}\cdot\hat{\mathbf{e}})^2, \qquad (1)$$

where the product $\hat{\mathbf{d}}\cdot\hat{\mathbf{e}}$ represents the projection of the polarization vector $\hat{\mathbf{e}}$ of the excitation light on the unit vector of the

molecular dipole $\hat{\mathbf{d}}$ and λ denotes the excitation wavelength. Γ is the lifetime-limited linewidth and Γ_{hom} the homogeneously broadened linewidth of the 00ZPL, respectively. If the molecular dipole is aligned with the polarization of the excitation light and the homogeneous broadening is negligible, the absorption cross section will approach that of a simple two-level atom and is comparable to the effective mode area A_{eff} [55] of our optical nanofiber of about $0.4\lambda^2$ (see Appendix B). This ensures a strong effect of a single molecule on the light field. The probability of a terrylene molecule to decay to the triplet state after excitation rather than to the singlet ground state is very low and has experimentally been found to be $<10^{-5}$ at cryogenic temperatures [2,56]. To maintain sufficient light guiding capabilities of the nanofiber-crystal system for spectroscopy and to ensure that the crystal stays tightly adhered to the vertically mounted nanofiber, the crystals have to be on the order of a few hundred nanometers in size. Such nanocrystals are grown by a reprecipitation method [57] from an oversaturated solution of an 8×10^{-5} molar mixture of terrylene/*p*-terphenyl in toluene. The solution is heated until both compounds are dissolved and then isopropanol is added as a reprecipitation agent. This procedure results in terrylene-doped *p*-terphenyl crystals of platelet morphology as seen in Fig. 2(a), which shows a scanning electron microscope (SEM) image of such crystals deposited on a silicon substrate. The majority of crystals have base dimensions in the range of 200 to 2000 nm and a base width-to-height ratio of 2.5:1 to 5:1 as determined by atomic force microscopy (AFM) measurements. The single-crystalline nature of these crystals has been verified by performing selected-area electron-diffraction (SAED) measurements using a transmission electron microscope (TEM) [see Fig. 2(b)]. SAED also indicates that the substrate-supported crystal platelet base face is of (001) orientation; i.e., the crystal's *c* axis is perpendicular to the substrate. It is known that the dipole moment of the transition to the lowest electronically excited state in terrylene is linear and lies along the long axis of the molecule [53]. When inserted into a *p*-terphenyl crystal, the molecule's long axis and thus the dipole moment lie nearly parallel to the crystal's *c* axis and therefore in our configuration nearly perpendicular to the substrate.

A terrylene-doped *p*-terphenyl nanocrystal is deposited on the nanofiber by a drop-touch method: a drop of the suspension of doped *p*-terphenyl nanocrystals is briefly brought into contact with the nanofiber via a pipette. During this process, the transmission of the excitation laser and the fluorescence of the nanofiber is monitored with a power meter and a spectrometer, respectively. When a doped crystal has adhered to the nanofiber surface during the contact with the suspension droplet, a typical fluorescence signal and some loss in transmission is observed. As crystals of a variety of sizes are produced during our growth process, we have to postselect the size of the deposited crystal. However, since the largest crystals sediment faster, we usually find suitably small ones in the suspension supernatant. If it is nevertheless found that the transmission deteriorates too much during the deposition process, the crystal can be washed off with acetone and another one deposited.

The TOF is mounted on a steel holder with two NdFeB magnets. This ensures that the fiber is firmly held and that it stays intact during the cooling process down to cryogenic temperatures. This fiber setup is mounted in the cold pot of
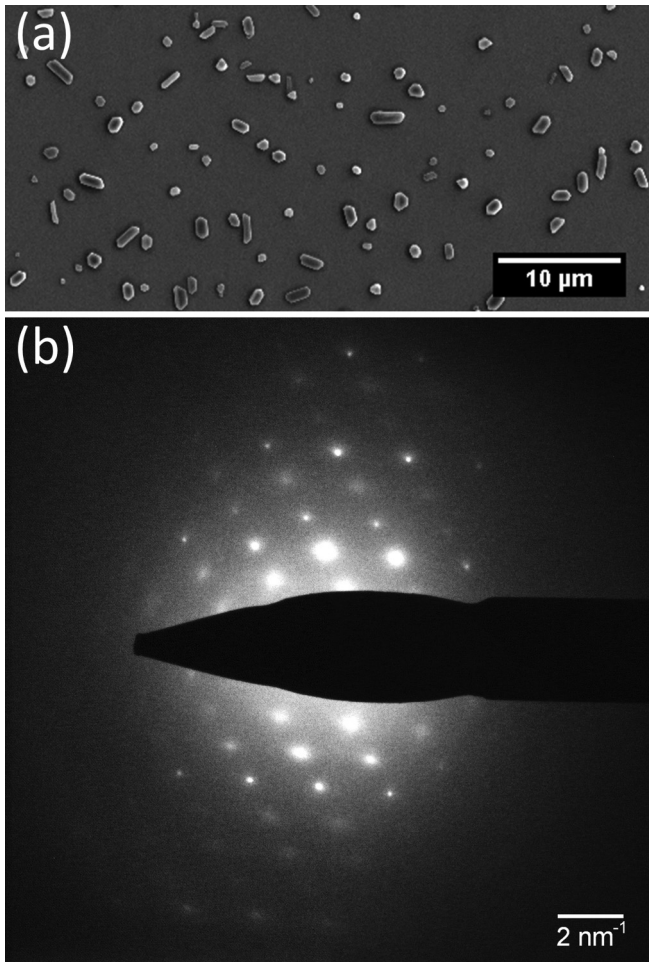
FIG. 2. (a) Scanning electron microscope image (FEI Quanta 200 FEG) of terrylene-doped *p*-terphenyl crystals on a silicon substrate. (b) Selected area electron diffraction pattern of an individual terrylene-doped *p*-terphenyl crystal (Philips CM200 TEM at 200 kV, imaged with the electron beam perpendicular to the crystal base face; exposure time was kept short to avoid electron-beam-induced degradation of the organic crystal [58]). The pattern is consistent with the monoclinic high-temperature phase of a single *p*-terphenyl single crystal [59] viewed along the [001] axis (considering double-diffraction effects, Cambridge Structural Database (CSD) entry terphe14).

a custom-made cryostat that can cool the sample to 4 K. To ensure efficient thermalization of the nanofiber and the crystal with the walls of the cold pot, helium buffer gas at a pressure of a few millibars is introduced into the cold pot before cooldown, after it has been evacuated.

To excite the molecules, light of a dye laser (Spectra-Physics Matisse-DS) is coupled into the optical fiber that connects to the TOF and that enters the cryostat via a Teflon feedthrough [Fig. 1(a)]. To compensate for intensity fluctuations and drifts, the laser beam is sent through an acousto-optic modulator (AOM) and partly onto a photodiode (PD) and is actively intensity stabilized. A fraction of the Stokes-shifted laser-induced fluorescence (LIF) of the molecule is collected by the nanofiber, is fiber-guided out of the cryostat, and can be monitored by a spectrometer (Shamrock SR-303i, Andor
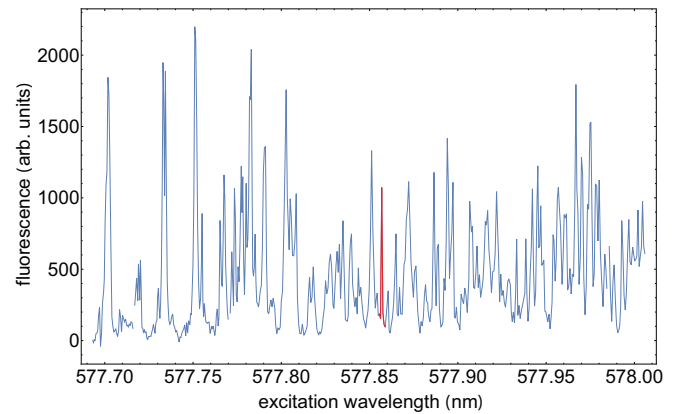

FIG. 3. Fluorescence excitation measurement of nanofiber-interfaced terrylene molecules. The red peak indicates the fluorescence of a single terrylene molecule.

Technology) or single-photon counting modules (SPCMs) at either end of the optical fiber. Contributions from the excitation light and fluorescence on the 00ZPL are filtered out by a long-pass (LP) filter. Together with a short-pass (SP) filter to block Raman scattering from the fiber, this leaves a transmission window in the range of 630 to 650 nm. Due to the inhomogeneous line shifts induced by the host crystal matrix, single molecules can be spectrally selected with the narrow-band dye laser if the terrylene concentration in the host crystal is small enough.

III. EXPERIMENTAL RESULTS

Figure 3 shows the fluorescence excitation spectrum of a molecular ensemble in the X4 orientation. The excitation line of what has been verified to be a single molecule is highlighted in red. To characterize the optical interface created by individual molecules and the optical nanofiber, we investigate several molecules that are located in the same nanocrystal. The transition frequencies of solid-state quantum emitters are known to be very sensitive to the environment, which can be a favorable effect if controlled well [60] or lead to unwanted spectral diffusion. In order to evaluate the stability of the transition frequency in our system, we record the same spectral line of the spectra of individual molecules over time. Figure 4 shows the evolution of a spectral line over the timescale of minutes. The excitation power corresponds to a saturation parameter of $I/I_S = 0.7$ and, over all spectra, the linewidth was measured to be 429 ± 20 MHz. A slow drift of 0.44 ± 0.14 MHz/s is observable. This could be a result of a drift in the laser frequency, the wavemeter, or the molecular transition frequency. The faster frequency scatter on top of this drift is found to be 18 MHz rms. This value is well below the lifetime-limited linewidth of the molecular transition (see Appendix A). Even for a lifetime-limited molecular spectrum and without any active stabilization this implies that the molecule would be resonant with a fixed-frequency laser for about 2 min. The measured stability of the molecule is thus found to be superior to other solid-state emitters, which may require active stabilization of the resonance frequency on a faster timescale [61,62]. By cooling the doped crystal to 1.7 K, we can also
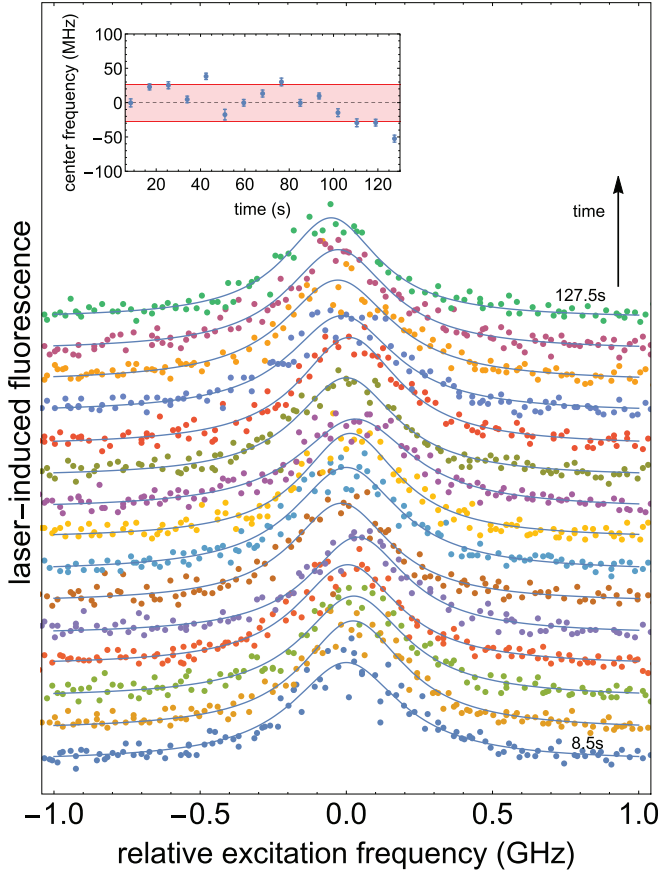
FIG. 4. Consecutive laser-induced fluorescence spectra of a single terrylene molecule coupled to an optical nanofiber. The individual scans are offset for clarity. Each scan takes 8.5 s. The inset explicitly shows the fitted resonance frequency as a function of time. The shaded region corresponds to the FWHM linewidth of a lifetime-limited molecular spectrum (see Appendix A).

achieve stable lifetime-limited spectra of our single molecules recorded on either end of the TOF, as is experimentally shown in Appendix A.

To verify the interaction with single quantum emitters, second-order fluorescence intensity correlation measurements are performed using a Hanbury-Brown–Twiss (HBT) setup [Fig. 1(a)]. The backscattered fluorescence is split by a 50:50 beam splitter (BS) and directed to two SPCMs. Their counts are then recorded by means of a field-programmable gate array and correlated. For a single quantum emitter, photon antibunching is observed, which manifests itself as an antibunching dip in the intensity correlation measurements at zero time delay τ between two detection events. Experimental imperfections such as incoherent background scatter will reduce the contrast of the dip but a dip deeper than 50% is proof of a single quantum emitter. Figure 5 shows second-order fluorescence intensity correlation measurements of a molecule on the nanofiber where the antibunching dip is clearly visible.

As the excitation intensity is increased, the onset of Rabi oscillations is apparent. Since the decay into the triplet state is negligible for short times, the measurements are fitted to the correlation function that is obtained by solving the optical Bloch equations for a two-level system with an overall
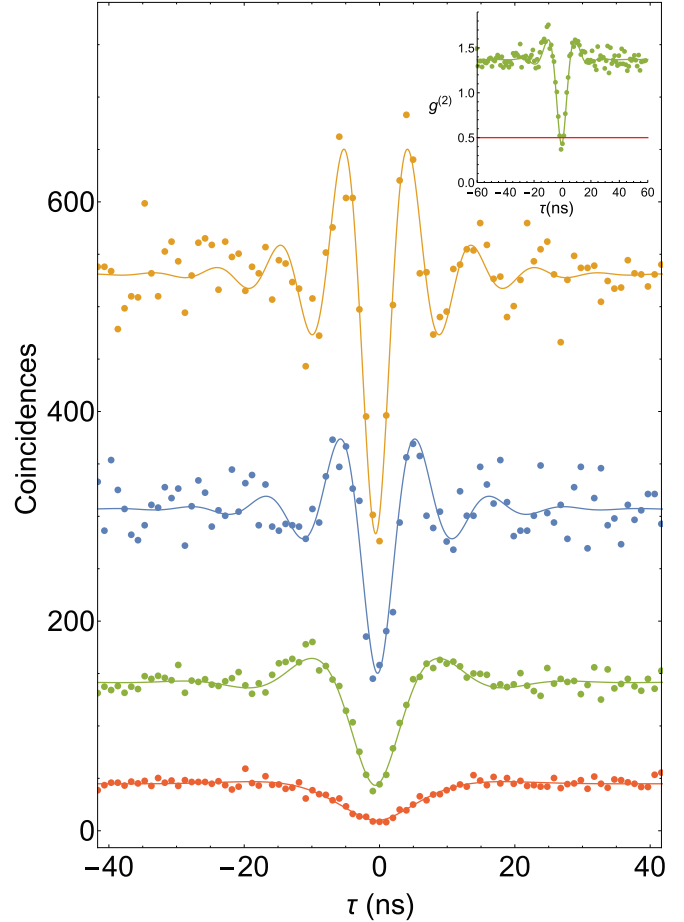

FIG. 5. Fluorescence intensity correlation measurements of molecule C for different excitation powers (from bottom to top: 0.7, 2.9, 7.4, and 11.1 nW). The coincidences were recorded for 1000 s and the time resolution for the data is 1 ns. With increasing excitation power, the onset of Rabi oscillations and an increase in incoherent background scatter is clearly seen. The inset shows the $g^{(2)}$ measurement at 2.9 nW normalized to the steady-state correlations of the fluorescence of the molecule, clearly indicating a single emitter.

amplitude A, a spontaneous decay rate Γ, and a Rabi frequency $\Omega = \mathbf{d} \cdot \mathbf{E}/\hbar$, where $\mathbf{d}$ is the dipole moment of the molecule's transition and $\mathbf{E}$ the electric field at the molecule's location [54]:

$$g^{(2)}(\tau) = A\left(1 - \left[\cos(\nu\tau) + \frac{3\Gamma}{4\nu}\sin(\nu\tau)\right]\exp\left(\frac{-3\Gamma\tau}{4}\right)\right)$$

with

$$\nu = \sqrt{\Omega^2 - \left(\frac{\Gamma}{4}\right)^2}. \qquad (2)$$

An incoherent Poissonian background B added to a signal with average intensity $\langle I\rangle$ reduces the contrast of the intensity correlation measurements. This is taken into account when analyzing our data with the modified intensity correlation function [63]

$$g_B^{(2)}(\tau) = 1 + \frac{\langle I\rangle^2}{(\langle I\rangle + B)^2}(g^2(\tau) - 1). \qquad (3)$$
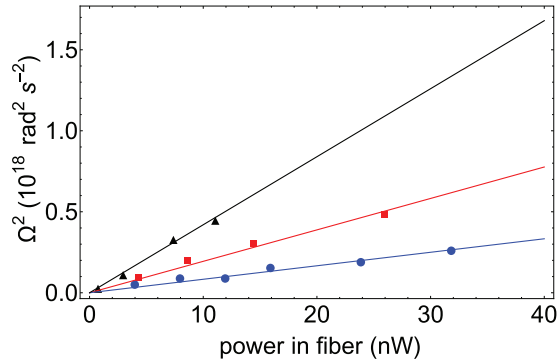
FIG. 6. Squared Rabi frequency as a function of excitation power for molecules A (red, squares), B (blue, circles), and C (black, triangles) and corresponding linear fits.

FIG. 7. Saturation of the resonant fluorescence intensity R_{LIF} as the excitation laser power is increased for molecules B (blue, circles) and D (green, diamonds) and corresponding fits.

We fit Eq. (3) to the data for different excitation powers while using Γ as a global fit parameter for all measurements on a given molecule. This yields the respective Rabi frequencies and the non-power-broadened homogeneous linewidth Γ of the molecule. From these fits we also obtain the saturation intensity I_S of the molecule as $I/I_S = 2\Omega^2/\Gamma^2$. Figure 6 shows this expected linear increase of the squared Rabi frequency as a function of excitation power for three different molecules in the same crystal. The error bars obtained from fitting the intensity correlation measurements are smaller than the depicted data points in Fig. 6. From the fits, the saturation power P_S corresponding to I_S is obtained. We obtain saturation powers for molecule A of $P_S = 1.8 \pm 0.3$ nW, for molecule B of $P_S = 4.3 \pm 0.8$ nW, and for molecule C of $P_S = 0.5 \pm 0.1$ nW. The biggest contribution to the error in the saturation powers arises from the uncertainty in determining the power in the fiber. We convert P_S to the maximum intensity at the surface of the nanofiber by considering the fundamental quasilinearly polarized HE_{11} mode that is supported by our optical nanofiber with a diameter of 320 nm [38]. Without the exact knowledge of the orientation of the molecule's transition dipole moment and its distance from the nanofiber surface, this gives an upper limit for the saturation intensity. The measured saturation intensities are $I_S < 1.8$ Wcm^{-2} for molecule A, $I_S < 4.3$ Wcm^{-2} for molecule B, and $I_S < 0.5$ Wcm^{-2} for molecule C. These results compare well with results obtained by other groups who studied terrylene in bulk p-terphenyl [42,64]. To our knowledge a saturation intensity of $I_S < 0.5$ Wcm^{-2} as for molecule C is the lowest measured so far for terrylene in p-terphenyl. As opposed to measurements on terrylene in bulk p-terphenyl using a confocal microscope, the excitation light in our case enters through the side of the thin host crystal platelets. As the transition dipole moment of the molecules lies nearly perpendicular to the base of these platelets, this suggests an improved overlap between the polarization of the nanofiber-guided excitation light and the transition dipole moment of the molecules. An independent measurement of the saturation power is obtained by recording the resonant fluorescence rate R_{LIF} as a function of excitation power as plotted in Fig. 7, which includes a fit to $R_{\mathrm{LIF}} = R_\infty \frac{P/P_S}{1+P/P_S}$. The error bars on the fluorescence rate that are obtained by taking the standard error of the amplitude from fits over several molecular spectra are smaller than the depicted data points. This measurement yields
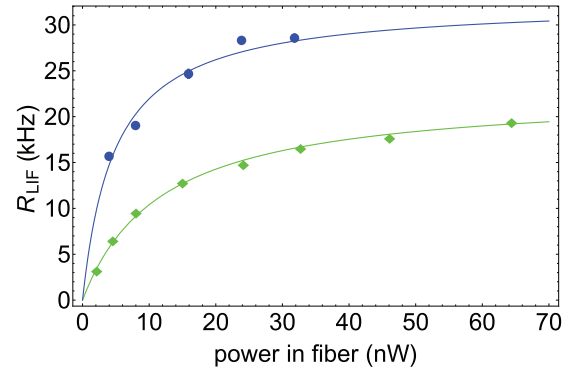
a saturation power of 4.8 ± 1.4 nW for molecule B, where the error stems from the fit and from the uncertainty in the excitation power inside the fiber. This translates into a saturation intensity of $I_S < 4.8$ Wcm^{-2} for molecule B in good agreement with $I_S < 4.3$ Wcm^{-2} as obtained with the HBT setup. We performed a further measurement on a fourth molecule (molecule D) that yielded a lower fluorescence rate and indeed was measured to have a higher saturation power of 11.4 ± 2.2 nW and therefore a saturation intensity of <11.4 Wcm^{-2}. This suggests that this molecule is located farther away from the nanofiber surface such that its fluorescence does not couple back to the nanofiber-guided modes as efficiently. Alternatively, the alignment between polarization of the excitation light and the dipole moment of molecule D may be less favorable. Although all molecules are embedded in a single crystal and therefore have the same orientation, the inherent birefringence of the host crystal can cause a less favorable alignment: The phase shift between the corresponding polarization components is $\Delta\phi = 2\pi \Delta n L/\lambda$, where λ is the vacuum wavelength, L the propagation distance, and Δn the effective birefringence, which can reach 0.32 in our case. The efficiency of exciting the different molecules is given by $\eta_{\mathrm{abs}} = \sigma/A_{\mathrm{eff}}(x,y)$, where $A_{\mathrm{eff}}(x,y)$ is the effective mode area at the position of the molecule. More details can be found in Appendix B. The molecules are also detected via the nanofiber interface and hence the overall efficiency for fluorescence excitation and detection via the nanofiber interface is then given as $\eta_{\mathrm{LIF}} = \eta_{\mathrm{abs}}\beta$, where $\beta = \Gamma_g/\Gamma_{\mathrm{sc}}$ is the coupling efficiency of dipole radiation to the nanofiber modes. This coupling efficiency depends on the radiated wavelength, distance, and orientation of the dipole with respect to the nanofiber surface. Here, Γ_g is the scattering rate into guided modes and Γ_{sc} is the total scattering rate of the dipole. For our case of a nanofiber with 160-nm radius and Stokes-shifted fluorescence in the range 630–650 nm, we calculated this coupling efficiency for a radially, azimuthally, and axially oriented dipole following [38] (see Fig. 8).

Since the power needed to saturate molecule C is the lowest yet measured for terrylene in p-terphenyl, we assume that this molecule is very close to the surface of the nanofiber. An upper limit for the other molecules from the nanofiber surface can then be estimated by comparing their saturation intensities. Because the host crystal is birefringent, we only give an upper
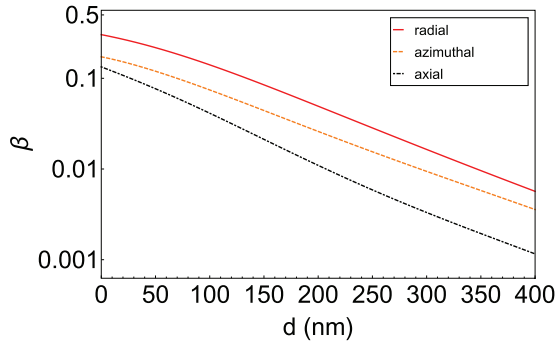
FIG. 8. Mean coupling efficiency of a linear radial (red), tangential (orange, dashed), and axial (black, dot-dashed) dipole, radiating at 630–650 nm, to the nanofiber as a function of distance from the nanofiber surface.

limit on the radial distance between the different molecules. Figure 9 shows the calculated efficiency of fluorescence excitation via the nanofiber interface for different positions of the dipole with respect to the nanofiber surface. The positions are chosen to lie within the volume of a platelet crystal with its base on the nanofiber surface. The molecular dipole is oriented perpendicular to the crystal's base and excited by quasilinearly polarized light via the nanofiber-based interface. Assuming unpolarized light instead of quasilinearly polarized light affects the relative distances between the different molecules by less than 3%. We did not incorporate the refractive indices of the crystal into this model because they would make the local efficiencies very dependent on the crystal's geometry and we are only interested in assigning the maximum radial distance of the measured molecules. The maximum radial distances of the investigated molecules are depicted in their respective
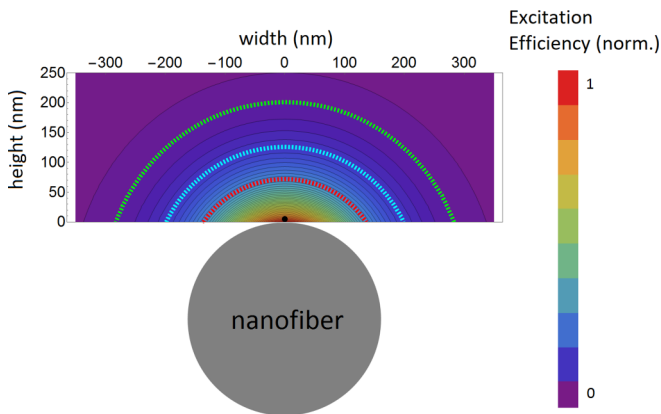

FIG. 9. The excitation efficiency η_{abs} for a molecular dipole at different positions with respect to the nanofiber. The spatial coordinates are chosen assuming a platelet crystal that is lying with its base on the nanofiber surface. The contact point of nanofiber and crystal is at the origin of this reference frame. The efficiency is normalized to the maximum excitation efficiency on the nanofiber surface of 17% (see Appendix B). The maximum radial distances for the different molecules are indicated by dashed colored lines (A, red; B, blue; and D, green, from bottom to top). The reference molecule C is shown as a black dot and is assumed to be located directly on the nanofiber surface at position $(x, y) = (0, 0)$.

colors by dashed contours (Fig. 9). These results show that they radially all lie within less than 481 nm of each other and less than 201 nm from the nanofiber surface. This translates into coupling efficiencies for a radial dipole to the nanofiber mode between 5% and 30% (Fig. 8). This means that our setup can be a superior choice for coupling single photons to single-mode optical fibers compared to using conventional confocal microscopes [65–67] and thus opens the way for fully fiber-coupled single-photon sources. It is also an important step towards strong coupling of single molecules to optical waveguide structures.

IV. CONCLUSION

Summarizing, we have shown how single molecules can be optically interfaced via the evanescent field surrounding an optical nanofiber. This is an important addition to the toolbox of quantum emitters such as atoms [34,68,69], quantum dots [33,65], and nitrogen-vacancy centers in nanodiamonds [41,70] that have been fiber integrated by coupling to optical nanofibers. Each of these systems has its own intrinsic advantages for their usage in quantum networks. Single molecules in solids are efficient quantum emitters that come in a large variety of emission wavelengths. This makes them suitable to be interfaced with other quantum emitters [1]. They have an advantageous level structure for the implementation of triggered single-photon sources [43,71] and have proven their versatility in quantum optics [72–74]. Further, single waveguide-coupled molecules allow the investigation of photon-mediated interactions between two quantum emitters even when they are separated by much more than the excitation wavelength [75–77]. These interactions can be further enhanced by using a nanofiber between two fiber Bragg gratings and thereby realizing a high-Q cavity [78]. Single molecules that are coupled to the evanescent field of optical nanofibers therefore not only offer a rich experimental platform for investigating entanglement and correlations between quantum emitters, they also provide a means for implementing components of quantum networks such as fiber-coupled single-photon sources [32,79,80] or photon sorters [81,82].

APPENDIX A: LIFETIME-LIMITED SINGLE PHOTONS FROM A FULLY FIBER-INTEGRATED SINGLE MOLECULE

To show that we can readily produce fiber-coupled lifetime-limited photons from single molecules in nanocrystals with our setup, we have measured molecular spectra and corresponding fluorescence correlation measurements at a temperature of 1.7 K. These measurements were performed on a different
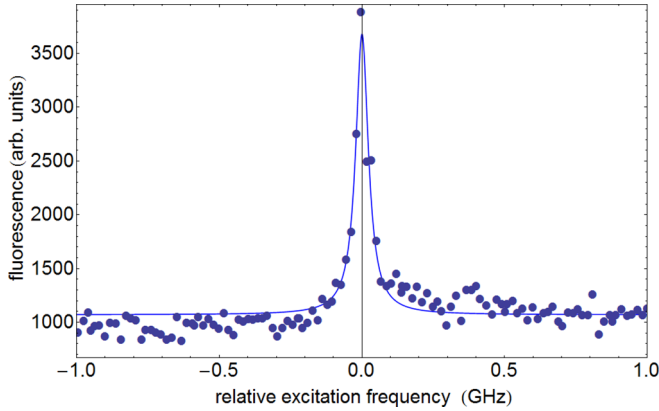
FIG. 10. Laser-induced fluorescence spectrum of a single terrylene molecule coupled to an optical nanofiber at a temperature of 1.7 K.

sample mounted in a helium flow cryostat (Janis) that can cool samples continuously below 2 K. Figure 10 shows a molecular spectrum at 1.7 K that has a linewidth of 54 ± 6 MHz and Fig. 11 shows the corresponding second-order fluorescence correlation measurement yielding a linewidth of 40 ± 22 MHz in agreement with that obtained from the spectrum. We can measure such spectra on both ends of the tapered optical fiber as shown in Fig. 12. This underpins the fully fiber-coupled nature of our single molecules.

APPENDIX B: EXCITATION EFFICIENCY OF A MOLECULE ON THE OPTICAL NANOFIBER SURFACE

The efficiency of exciting a molecule via the nanofiber interface is given by $\eta_{abs} = \sigma/A_{eff}(x,y)$, where $A_{eff}(x,y)$ is the effective mode area of the light field at the position of the molecule. Here, we want to estimate the excitation efficiency for a single molecule that is situated on the surface of the optical nanofiber at position $(x,y) = (0,0)$ (see Fig. 9 in main text) and has a radially oriented transition dipole moment with respect to the nanofiber. It is excited by a mode that is quasi-linearly polarized and for which the transverse polarization
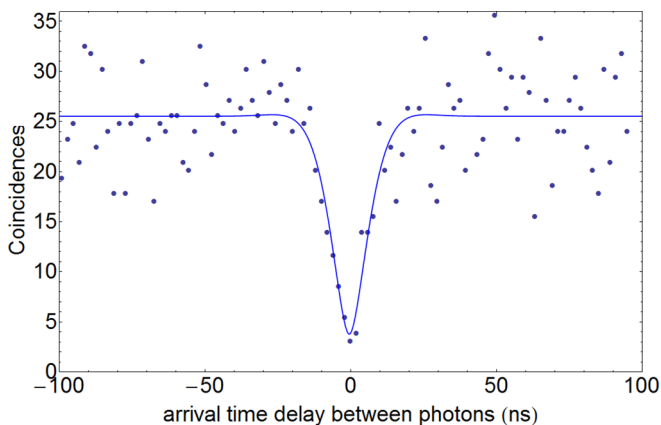

FIG. 11. Fluorescence intensity correlation measurements of a single terrylene molecule coupled to an optical nanofiber at a temperature of 1.7 K. The coincidences are analyzed in bins of 1000 s and the time resolution for the data is 2 ns.
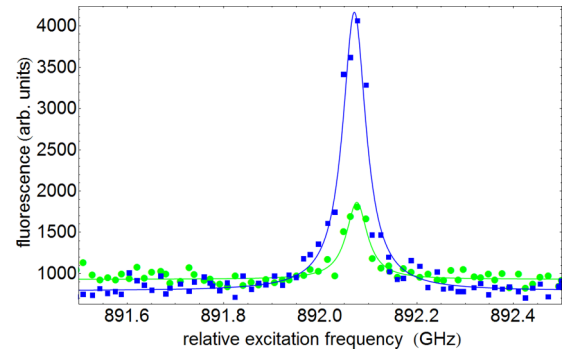

FIG. 12. Laser-induced fluorescence spectra of a single terrylene molecule coupled to an optical nanofiber at a temperature of 1.7 K observed from both sides of the optical fiber. The fit to the spectra reveals a linewidth (FWHM) of 52.5 ± 5.1 MHz (blue, squares) and 58.6 ± 2.7 MHz (green, circles). The difference in signal height of the two spectra may stem from the possibly asymmetric position of the molecule inside the crystal with respect to the forward- and backward-propagation direction of laser-induced fluorescence in the optical nanofiber.

component is aligned with the direction of the molecule's dipole moment. The effective mode area on the surface is then given as $A_{eff,surf} = P/(I_{surf}\,(\hat{\mathbf{d}} \cdot \hat{\mathbf{e}}_{surf})^2)$, where I_{surf} is the surface intensity at $(0,0)$ and $\hat{\mathbf{d}} \cdot \hat{\mathbf{e}}_{surf}$ is the overlap between the unit vector of the molecular dipole moment and the polarization vector at the position of the molecule. On the surface this then yields an effective mode area of $0.4\lambda^2$, with an excitation wavelength of 580 nm and for a nanofiber with a diameter of 320 nm. We deduce a value for the absorption cross section of the molecule from our saturation intensity measurements. The saturation intensity of the molecule closest to the nanofiber has been $I_S < 0.5$ Wcm^{-2}. The intensity needed to saturate a molecular transition depends on its molecular dipole moment as [8]

$$I_S = \epsilon_0 c \hbar^2 \frac{k_{21} + k'_{23} + k''_{23}}{|\mathbf{d}|^2 (2 + A) T_2}. \qquad \text{(B1)}$$

Here, to obtain a correct value for the magnitude of the dipole moment $\mathbf{d}$, the metastable triplet state, which is split into two levels without an external field, has to be taken into account. In this case, $A = k'_{23}/k'_{31} + k''_{23}/k''_{31}$. k_{ij} are the transition rates from level i to level j and the superscripts $'$ and $''$ represent the two nondegenerate levels of the triplet level 3. $1/T_2$ represents the total dephasing rate of the excited state. Using Eq. (B1) and the triplet-state parameters for terrylene in p-terphenyl from [83], we obtain $|\mathbf{d}| > 4.1$ Debye for the transition dipole moment of terrylene in p-terphenyl from the ground state to the first electronically excited state. The molecular dipole moment $\mathbf{d} = -e\mathbf{r}$ yields a minimum oscillator strength for this transition as [84]

$$f = \frac{2m\omega}{3\hbar}|\mathbf{r}|^2 = 0.14. \qquad \text{(B2)}$$

This gives an effective absorption cross section of $\sigma = 0.14 \times 3\lambda^2/(2\pi)$ and hence an excitation probability of a single molecule on the nanofiber surface of 17%.

[1] P. Siyushev, G. Stein, J. Wrachtrup, and I. Gerhardt, Molecular photons interfaced with alkali atoms, Nature (London) **509**, 66 (2014).

[2] T. Basché, S. Kummer, and C. Bräuchle, Direct spectroscopic observation of quantum jumps of a single molecule, Nature (London) **373**, 132 (1995).

[3] T. Basché, W. E. Moerner, M. Orrit, and H. Talon, Photon Antibunching in the Fluorescence of a Single Dye Molecule Trapped in a Solid, Phys. Rev. Lett. **69**, 1516 (1992).

[4] M. Celebrano, P. Kukura, A. Renn, and V. Sandoghdar, Single-molecule imaging by optical absorption, Nat. Photonics **5**, 95 (2011).

[5] I. Gerhardt, G. Wrigge, P. Bushev, G. Zumofen, M. Agio, R. Pfab, and V. Sandoghdar, Strong Extinction of a Laser Beam by a Single Molecule, Phys. Rev. Lett. **98**, 033601 (2007).

[6] I. Gerhardt, G. Wrigge, J. Hwang, G. Zumofen, and V. Sandoghdar, Coherent nonlinear single-molecule microscopy, Phys. Rev. A **82**, 063823 (2010).

[7] B. Kozankiewicz and M. Orrit, Single-molecule photophysics, from cryogenic to ambient conditions, Chem. Soc. Rev. **43**, 1029 (2014).

[8] F. Jelezko and J. Wrachtrup, Read-out of single spins by optical spectroscopy, J. Phys.: Condens. Matter **16**, R1089 (2004).

[9] P. C. Maurer, G. Kucsko, C. Latta, L. Jiang, N. Y. Yao, S. D. Bennett, F. Pastawski, D. Hunger, N. Chisholm, M. Markham, D. J. Twitchen, J. I. Cirac, and M. D. Lukin, Room-temperature quantum bit memory exceeding one second, Science **336**, 1283 (2012).

[10] P. Neumann, N. Mizuochi, F. Rempp, P. Hemmer, H. Watanabe, S. Yamasaki, V. Jacques, T. Gaebel, F. Jelezko, and J. Wrachtrup, Multipartite entanglement among single spins in diamond, Science **320**, 1326 (2008).

[11] B. Pingault, J. N. Becker, C. H. H. Schulte, C. Arend, C. Hepp, T. Godde, A. I. Tartakovskii, M. Markham, C. Becher, and M. Atatüre, All-Optical Formation of Coherent Dark States of Silicon-Vacancy Spins in Diamond, Phys. Rev. Lett. **113**, 263601 (2014).

[12] J. Hansom, C. H. H. Schulte, C. Le Gall, C. Matthiesen, E. Clarke, M. Hugues, J. M. Taylor, and M. Atatüre, Environment-assisted quantum control of a solid-state spin via coherent dark states, Nat. Phys. **10**, 725 (2014).

[13] A. Delteil, Z. Sun, W. Gao, E. Togan, S. Faelt, and A. Imamoğlu, Generation of heralded entanglement between distant hole spins, Nat. Phys. **12**, 218 (2016).

[14] R. Yalla, M. Sadgrove, K. P. Nayak, and K. Hakuta, Cavity Quantum Electrodynamics on a Nanofiber Using a Composite Photonic Crystal Cavity, Phys. Rev. Lett. **113**, 143601 (2014).

[15] M. Arcari, I. Söllner, A. Javadi, S. L. Hansen, S. Mahmoodian, J. Liu, H. Thyrrestrup, E. H. Lee, J. D. Song, S. Stobbe, and P. Lodahl, Near-Unity Coupling Efficiency of a Quantum Emitter to a Photonic Crystal Waveguide, Phys. Rev. Lett. **113**, 093603 (2014).

[16] A. Javadi, I. Söllner, M. Arcari, S. L. Hansen, L. Midolo, S. Mahmoodian, G. Kiršanskė, T. Pregnolato, E. H. Lee, J. D. Song, S. Stobbe, and P. Lodahl, Single-photon non-linear optics with a quantum dot in a waveguide, Nat. Commun. **6**, 8655 (2015).

[17] K. Nemoto, M. Trupke, S. J. Devitt, A. M. Stephens, B. Scharfenberger, K. Buczak, T. Nöbauer, M. S. Everitt, J. Schmiedmayer, and W. J. Munro, Photonic Architecture for Scalable Quantum Information Processing in Diamond, Phys. Rev. X **4**, 031022 (2014).

[18] H. J. Kimble, The quantum internet, Nature (London) **453**, 1023 (2008).

[19] M. W. Doherty, V. V. Struzhkin, D. A. Simpson, L. P. McGuinness, Y. Meng, A. Stacey, T. J. Karle, R. J. Hemley, N. B. Manson, L. C. L. Hollenberg, and S. Prawer, Electronic Properties and Metrology Applications of the Diamond NV$^-$ Center under Pressure, Phys. Rev. Lett. **112**, 047601 (2014).

[20] G. Goldstein, P. Cappellaro, J. R. Maze, J. S. Hodges, L. Jiang, A. S. Sørensen, and M. D. Lukin, Environment-Assisted Precision Measurement, Phys. Rev. Lett. **106**, 140502 (2011).

[21] V. M. Acosta, K. Jensen, C. Santori, D. Budker, and R. G. Beausoleil, Electromagnetically Induced Transparency in a Diamond Spin Ensemble Enables All-Optical Electromagnetic Field Sensing, Phys. Rev. Lett. **110**, 213605 (2013).

[22] S. Faez, S. J. van der Molen, and M. Orrit, Optical tracing of multiple charges in single-electron devices, Phys. Rev. B **90**, 205405 (2014).

[23] G. Mazzamuto, A. Tabani, S. Pazzagli, S. Rizvi, A. Reserbat-Plantey, K. Schädler, G. Navickaite, L. Gaudreau, F. S. Cataliotti, F. Koppens, and C. Toninelli, Single-molecule study for a graphene-based nano-position sensor, New J. Phys. **16**, 113007 (2014).

[24] G. Kucsko, P. C. Maurer, N. Y. Yao, M. Kubo, H. J. Noh, P. K. Lo, H. Park, and M. D. Lukin, Nanometre-scale thermometry in a living cell, Nature (London) **500**, 54 (2013).

[25] M. D. Lukin and A. Imamoğlu, Controlling photons using electromagnetically induced transparency, Nature (London) **413**, 273 (2001).

[26] K. F. Reim, J. Nunn, V. O. Lorenz, B. J. Sussman, K. C. Lee, N. K. Langford, D. Jaksch, and I. A. Walmsley, Towards high-speed optical quantum memories, Nat. Photonics **4**, 218 (2010).

[27] J. Volz, M. Scheucher, C. Junge, and A. Rauschenbeutel, Nonlinear π phase shift for single fibre-guided photons interacting with a single resonator-enhanced atom, Nat. Photonics **8**, 965 (2014).

[28] J. D. Thompson, T. G. Tiecke, N. P. de Leon, J. Feist, A. V. Akimov, M. Gullans, A. S. Zibrov, V. Vuletić, and M. D. Lukin, Coupling a single trapped atom to a nanoscale optical cavity, Science **340**, 1202 (2013).

[29] S. Ritter, C. Nölleke, C. Hahn, A. Reiserer, A. Neuzner, M. Uphoff, M. Mücke, E. Figueroa, J. Bochmann, and G. Rempe, An elementary quantum network of single atoms in optical cavities, Nature (London) **484**, 195 (2012).

[30] S. Schietinger, T. Schröder, and O. Benson, One-by-one coupling of single defect centers in nanodiamonds to high-Q modes of an optical microresonator, Nano Lett. **8**, 3911 (2008).

[31] S. Faez, P. Türschmann, H. R. Haakh, S. Götzinger, and V. Sandoghdar, Coherent Interaction of Light and Single Molecules in a Dielectric Nanoguide, Phys. Rev. Lett. **113**, 213601 (2014).

[32] J. Hwang and E. A. Hinds, Dye molecules as single-photon sources and large optical nonlinearities on a chip, New J. Phys. **13**, 085009 (2011).

[33] R. Yalla, F. L. Kien, M. Morinaga, and K. Hakuta, Efficient Channeling of Fluorescence Photons from Single Quantum Dots into Guided Modes of Optical Nanofiber, Phys. Rev. Lett. **109**, 063602 (2012).

[34] E. Vetsch, D. Reitz, G. Sagué, R. Schmidt, S. T. Dawkins, and A. Rauschenbeutel, Optical Interface Created by Laser-Cooled

Atoms Trapped in the Evanescent Field Surrounding an Optical Nanofiber, Phys. Rev. Lett. **104**, 203603 (2010).

[35] G. Kiršanskė, H. Thyrrestrup, R. S. Daveau, C. L. Dreeßen, T. Pregnolato, L. Midolo, P. Tighineanu, A. Javadi, S. Stobbe, R. Schott, A. Ludwig, A. D. Wieck, S. I. Park, J. D. Song, A. V. Kuhlmann, I. Söllner, M. C. Löbl, R. J. Warburton, and P. Lodahl, Indistinguishable and efficient single photons from a quantum dot in a planar nanobeam waveguide, Phys. Rev. B **96**, 165306 (2017).

[36] P. E. Lombardi, A. P. Ovvyan, S. Pazzagli, G. Mazzamuto, G. Kewes, O. Neitzke, N. Gruhler, O. Benson, W. H. P. Pernice, F. S. Cataliotti, and C. Toninelli, Photostable molecules on chip: Integrated sources of nonclassical light, ACS Photonics **5**, 126 (2018).

[37] R. Garcia-Fernandez, W. Alt, F. Bruse, C. Dan, K. Karapetyan, O. Rehband, A. Stiebeiner, U. Wiedemann, D. Meschede, and A. Rauschenbeutel, Optical nanofibers and spectroscopy, Appl. Phys. B **105**, 3 (2011).

[38] F. L. Kien, S. D. Gupta, V. I. Balykin, and K. Hakuta, Spontaneous emission of a cesium atom near a nanofiber: Efficient coupling of light to guided modes, Phys. Rev. A **72**, 032509 (2005).

[39] D. Reitz, C. Sayrin, R. Mitsch, P. Schneeweiss, and A. Rauschenbeutel, Coherence Properties of Nanofiber-Trapped Cesium Atoms, Phys. Rev. Lett. **110**, 243603 (2013).

[40] K. P. Nayak, P. N. Melentiev, M. Morinaga, F. L. Kien, V. I. Balykin, and K. Hakuta, Optical nanofiber as an efficient tool for manipulating and probing atomic fluorescence, Opt. Express **15**, 5431 (2007).

[41] L. Liebermeister, F. Petersen, A. v. Münchow, D. Burchardt, J. Hermelbracht, T. Tashima, A. W. Schell, O. Benson, T. Meinhardt, A. Krueger, A. Stiebeiner, A. Rauschenbeutel, H. Weinfurter, and M. Weber, Tapered fiber coupling of single photons emitted by a deterministically positioned single nitrogen vacancy center, Appl. Phys. Lett. **104**, 031101 (2014).

[42] S. Kummer, T. Basché, and C. Bräuchle, Terrylene in *p*-terphenyl: A novel single crystalline system for single molecule spectroscopy at low temperatures, Chem. Phys. Lett. **229**, 309 (1994).

[43] W. E. Moerner, Single-photon sources based on single molecules in solids, New J. Phys. **6**, 88 (2004).

[44] W. E. Moerner and M. Orrit, Illuminating single molecules in condensed matter, Science **283**, 1670 (1999).

[45] J. Michaelis, C. Hettich, A. Zayats, B. Eiermann, J. Mlynek, and V. Sandoghdar, A single molecule as a probe of optical intensity distribution, Opt. Lett. **24**, 581 (1999).

[46] Ph. Tamarat, A. Maali, B. Lounis, and M. Orrit, Ten years of single-molecule spectroscopy, J. Phys. Chem. A **104**, 1 (2000).

[47] P. Türschmann, N. Rotenberg, J. Renger, I. Harder, O. Lohse, T. Utikal, S. Götzinger, and V. Sandoghdar, On-chip linear and nonlinear control of single molecules coupled to a nanoguide, Nano Lett. **17**, 4941 (2017).

[48] D. Wang, H. Kelkar, D. Martin-Cano, T. Utikal, S. Götzinger, and V. Sandoghdar, Coherent Coupling of a Single Molecule to a Scanning Fabry-Pérot Microcavity, Phys. Rev. X **7**, 021014 (2017).

[49] A. Chizhik, F. Schleifenbaum, R. Gutbrod, A. Chizhik, D. Khoptyar, A. J. Meixner, and J. Enderlein, Tuning the Fluorescence Emission Spectra of a Single Molecule with a Variable Optical Subwavelength Metal Microcavity, Phys. Rev. Lett. **102**, 073002 (2009).

[50] D. J. Norris, M. Kuwata-Gonokami, and W. E. Moerner, Excitation of a single molecule on the surface of a spherical microcavity, Appl. Phys. Lett. **71**, 297 (1997).

[51] F. Warken, A. Rauschenbeutel, and T. Bartholomaus, Fiber pulling profits from precise positioning: Precise motion control improves manufacturing of fiber optical resonators, Photonics Spectra **42**, 73 (2008).

[52] A. Stiebeiner, R. Garcia-Fernandez, and A. Rauschenbeutel, Design and optimization of broadband tapered optical fibers with a nanofiber waist, Opt. Express **18**, 22677 (2010).

[53] P. Bordat and R. Brown, Molecular mechanisms of photo-induced spectral diffusion of single terrylene molecules in *p* terphenyl, J. Chem. Phys. **116**, 229 (2002).

[54] R. Loudon, *The Quantum Theory of Light* (Oxford University Press, Oxford, 2000).

[55] F. Warken, E. Vetsch, D. Meschede, M. Sokolowski, and A. Rauschenbeutel, Ultra-sensitive surface absorption spectroscopy using sub-wavelength diameter optical fibers, Opt. Express **15**, 11952 (2007).

[56] M. Banasiewicz, O. Morawski, D. Wicek, and B. Kozankiewicz, Triplet population and depopulation rates of single terrylene molecules in *p*-terphenyl crystal, Chem. Phys. Lett. **414**, 374 (2005).

[57] H. Kasai, H. S. Nalwa, H. Oikawa, S. Okada, H. Matsuda, N. Minami, A. Kakuta, K. Ono, A. Mukoh, and H. Nakanishi, A novel preparation method of organic microcrystals, Jpn. J. Appl. Phys. **31**, L1132 (1992).

[58] P. Li and R. F. Egerton, Radiation damage in coronene, rubrene and *p*-terphenyl, measured for incident electrons of kinetic energy between 100 and 200 keV, Ultramicroscopy **101**, 161 (2004).

[59] A. P. Rice, F. S. Tham, and E. L. Chronister, A temperature dependent x-ray study of the order-disorder enantiotropic phase transition of *p*-terphenyl, J. Chem. Crystallogr. **43**, 14 (2012).

[60] F. Dolde, H. Fedder, M. W. Doherty, T. Nöbauer, F. Rempp, G. Balasubramanian, T. Wolf, F. Reinhard, L. C. L. Hollenberg, F. Jelezko, and J. Wrachtrup, Electric-field sensing using single diamond spins, Nat. Phys. **7**, 459 (2011).

[61] L. Robledo, H. Bernien, I. van Weperen, and R. Hanson, Control and Coherence of the Optical Transition of Single Nitrogen Vacancy Centers in Diamond, Phys. Rev. Lett. **105**, 177403 (2010).

[62] J. Hansom, C. H. H. Schulte, C. Matthiesen, M. J. Stanley, and M. Atatüre, Frequency stabilization of the zero-phonon line of a quantum dot via phonon-assisted active feedback, Appl. Phys. Lett. **105**, 172107 (2014).

[63] R. Verberk and M. Orrit, Photon statistics in the fluorescence of single molecules and nanocrystals: Correlation functions versus distributions of on- and off-times, J. Chem. Phys. **119**, 2214 (2003).

[64] Ph. Tamarat, B. Lounis, J. Bernard, M. Orrit, S. Kummer, R. Kettner, S. Mais, and T. Basché, Pump-Probe Experiments with a Single Molecule: ac-Stark Effect and Nonlinear Optical Response, Phys. Rev. Lett. **75**, 1514 (1995).

[65] M. Fujiwara, K. Toubaru, T. Noda, H. Zhao, and S. Takeuchi, Highly efficient coupling of photons from nanoemitters into single-mode optical fibers, Nano Lett. **11**, 4362 (2011).

[66] T. Schröder, F. Gädeke, M. J. Banholzer, and O. Benson, Ultrabright and efficient single-photon generation based on nitrogen-vacancy centres in nanodiamonds on a solid immersion lens, New J. Phys. **13**, 055017 (2011).

[67] J. Karlsson, L. Rippe, and S. Kröll, A confocal optical microscope for detection of single impurities in a bulk crystal at cryogenic temperatures, Rev. Sci. Instrum. **87**, 033701 (2016).

[68] A. Goban, K. S. Choi, D. J. Alton, D. Ding, C. Lacroûte, M. Pototschnig, T. Thiele, N. P. Stern, and H. J. Kimble, Demonstration of a State-Insensitive, Compensated Nanofiber Trap, Phys. Rev. Lett. **109**, 033603 (2012).

[69] M. Hafezi, Z. Kim, S. L. Rolston, L. A. Orozco, B. L. Lev, and J. M. Taylor, Atomic interface between microwave and optical photons, Phys. Rev. A **85**, 020302 (2012).

[70] M. Fujiwara, H. Zhao, T. Noda, K. Ikeda, H. Sumiya, and S. Takeuchi, Ultrathin fiber-taper coupling with nitrogen vacancy centers in nanodiamonds at cryogenic temperatures, Opt. Lett. **40**, 5702 (2015).

[71] B. Lounis and W. E. Moerner, Single photons on demand from a single molecule at room temperature, Nature (London) **407**, 491 (2000).

[72] J. Hwang, M. Pototschnig, R. Lettow, G. Zumofen, A. Renn, S. Götzinger, and V. Sandoghdar, A single-molecule optical transistor, Nature (London) **460**, 76 (2009).

[73] M. Pototschnig, Y. Chassagneux, J. Hwang, G. Zumofen, A. Renn, and V. Sandoghdar, Controlling the Phase of a Light Beam with a Single Molecule, Phys. Rev. Lett. **107**, 063001 (2011).

[74] A. Maser, B. Gmeiner, T. Utikal, S. Götzinger, and V. Sandoghdar, Few-photon coherent nonlinear optics with a single molecule, Nat. Photonics **10**, 450 (2016).

[75] S. Rist, J. Eschner, M. Hennrich, and G. Morigi, Photon-mediated interaction between two distant atoms, Phys. Rev. A **78**, 013808 (2008).

[76] A. F. van Loo, A. Fedorov, K. Lalumière, B. C. Sanders, A. Blais, and A. Wallraff, Photon-mediated interactions between distant artificial atoms, Science **342**, 1494 (2013).

[77] F. L. Kien, S. D. Gupta, K. P. Nayak, and K. Hakuta, Nanofiber-mediated radiative transfer between two distant atoms, Phys. Rev. A **72**, 063815 (2005).

[78] C. Wuttke, M. Becker, S. Brückner, M. Rothhardt, and A. Rauschenbeutel, Nanofiber Fabry-Pérot microresonator for nonlinear optics and cavity quantum electrodynamics, Opt. Lett. **37**, 1949 (2012).

[79] V. Ahtee, R. Lettow, R. Pfab, A. Renn, E. Ikonen, S. Gotzinger, and V. Sandoghdar, Molecules as sources for indistinguishable single photons, J. Mod. Opt. **56**, 161 (2009).

[80] C. Polisseni, K. D. Major, S. Boissier, S. Grandi, A. S. Clark, and E. A. Hinds, Stable, single-photon emitter in a thin organic crystal for application to quantum-photonic devices, Opt. Express **24**, 5615 (2016).

[81] D. Witthaut, M. D. Lukin, and A. S. Sørensen, Photon sorters and QND detectors using single photon emitters, Europhys. Lett. **97**, 50007 (2012).

[82] T. C. Ralph, I. Söllner, S. Mahmoodian, A. G. White, and P. Lodahl, Photon Sorting, Efficient Bell Measurements, and a Deterministic Controlled-*Z* Gate Using a Passive Two-Level Nonlinearity, Phys. Rev. Lett. **114**, 173603 (2015).

[83] G. C. Hegerfeldt and D. Seidel, Blinking molecules: Determination of photophysical parameters from the intensity correlation function, J. Chem. Phys. **118**, 7741 (2003).

[84] B. H. Bransden and C. J. Joachain, *Physics of Atoms and Molecules* (Prentice Hall, Englewood Cliffs, NJ, 2003).